Cylindrical acoustical holography applied to full-scale jet noise

Alan T. Wall,[a] Kent L. Gee, Tracianne B. Neilsen, and David W. Krueger
Brigham Young University, Provo, Utah 84602

Michael M. James
Blue Ridge Research and Consulting, Asheville, North Carolina 28801

(Received 26 March 2014; revised 9 July 2014; accepted 11 July 2014)

Near-field acoustical holography methods are used to predict sound radiation from an engine installed on a high-performance military fighter aircraft. Cylindrical holography techniques are an efficient approach to measure the large and complex sound fields produced by full-scale jets. It is shown that a ground-based, one-dimensional array of microphones can be used in conjunction with a cylindrical wave function field representation to provide a holographic reconstruction of the radiated sound field at low frequencies. In the current work, partial field decomposition methods and numerical extrapolation of data beyond the boundaries of the hologram aperture are required prior to holographic projection. Predicted jet noise source distributions and directionality are shown for four frequencies between 63 and 250 Hz. It is shown that the source distribution narrows and moves upstream, and that radiation directionality shifts toward the forward direction, with increasing frequency. A double-lobe feature of full-scale jet radiation is also demonstrated.
 [http://dx.doi.org/10.1121/1.4892755]

PACS number(s): 43.50.Nm, 43.60.Sx, 43.40.Sk, 43.28.Ra [EGW] Pages: 1120–1128

I. INTRODUCTION

For more than six decades, the jet aeroacoustics community has sought to predict and measure source distributions and noise emissions from jets. The last decade has seen investigations into the use of near-field acoustical holography (NAH) to the jet noise problem (Lee and Bolton, 2007; Shah *et al.*, 2011; Wall *et al.*, 2012a). The various implementations of NAH represent sound fields as superpositions of elementary wave functions that satisfy the Helmholtz equation, and perform optimized fits of these functions to data measured over an extended microphone array, or "hologram." The weighted functions are evaluated at a desired location within the three-dimensional region in the vicinity of the hologram, which provides a reconstruction of the radiated sound field. It is often desirable to reconstruct the field at the source to generate an equivalent source model.

Because a successful NAH reconstruction requires that the radiating source region be sufficiently covered in extent to capture all the critical wave functions within the hologram, the source geometry guides the design of the hologram array. In turn, the source and hologram geometries guide the selection of wave functions. For example, the near field of an extended, flat vibrator is most conveniently measured with a two-dimensional array of microphones over a planar region, and most efficiently represented by an orthogonal set of plane waves. In the current study, the noise radiation from of a full-scale jet was measured by a one-dimensional array running parallel to the axial centerline of the jet, and the field is represented by cylindrical wave functions centered on the jet axis.

The dominant component of military jet noise is the highly directional, low-frequency radiation from convecting turbulence structures (Viswanathan, 2007; Gee *et al.*, 2013). These structures are formed from instabilities between the higher velocity fluid that exits a nozzle and the lower velocity ambient fluid. The structures grow as they propagate downstream, fed by the transition of the high-velocity (nominally uniform) fluid in the potential core into random-velocity turbulence (McInerny *et al.*, 2004), then decay away after the end of the core (Tam *et al.*, 2006; Schlinker *et al.*, 2007). The evolving turbulence structures result in a noise source that is partially coherent, i.e., that is characterized by coherence that decreases with distance from any point within the jet (Michalke, 1977; Fuchs and Michel, 1978; Michel, 2009). The sound field is also partially spatially coherent (Harker *et al.*, 2013; Viswanathan, 2007). Since NAH requires the use of a coherent hologram, partial field decomposition (PFD) methods are required (Hald, 1989), which methods rely on the theory of principal component analysis (Otte *et al.*, 1988) to represent mixed fields as the energetic summation of mutually incoherent partial fields (PFs). In several previous jet noise studies this process was called proper orthogonal decomposition (Arndt *et al.*, 1997; Suzuki and Colonius, 2006).

Previously, measurements with a planar hologram array were used to perform an NAH reconstruction of a full-scale jet on a military fighter aircraft (Wall *et al.*, 2012a). Plane waves were the elementary functions used in the NAH field representation. A plane wave model of the field resulted in a reconstruction that demonstrated the source directivity, but not the geometrical spreading that would result in reasonable source level estimates, i.e., the reconstructed levels did not increase from the hologram to the source region as much as

[a]Author to whom correspondence should be addressed. Current address: Air Force Research Laboratory, Battlespace Acoustics Branch, Wright-Patterson AFB, Dayton, OH 45433. Electronic mail: alantwall@gmail.com

would be expected from a cylindrical or spherical source. In addition, the hologram array in the previous planar NAH study could not be placed closer to the jet than about 4 m because of the high peak levels and transducer limitations (Wall *et al.*, 2012b). Hence, it is likely that the near-field evanescent (exponentially decaying) waves were not captured. Any evanescent information must also have been filtered out in the stringent regularization (Williams, 2001) that was applied to the data prior to projection. This, combined with the limited azimuthal coverage of the source, made plane waves an inefficient model for representing geometrical spreading. A preliminary investigation in the same study (Wall *et al.*, 2012a) demonstrated that cylindrical NAH can be used to represent a geometrically spreading sound field, even in the absence of evanescent waves.

The importance of evanescent wave components in the full-scale jet near field is not yet clear, but in a recent study of supersonic jets by Kuo *et al.* (2013), it was demonstrated that the acoustic (propagating) components of the spectra dominate the near field in the upstream region where convective turbulence velocities are supersonic, and the hydrodynamic (evanescent) components dominate downstream where the local convective velocities become subsonic. The competing components of acoustic and hydrodynamic pressures in the near field of a full-scale jet, and their relation to the geometrical spreading in the transition region from the near to the far field, are worth further investigation. This would require the use of pressure sensors that could measure the high peak pressures that exist in the near field (Wall *et al.*, 2012b). For all studies performed with the current data set, including the present paper, it may be that the source reconstructions represent only the radiating (supersonic source) energies.

In this paper it is shown that cylindrical NAH using a one-dimensional ground-based array of microphones is a convenient method to perform field reconstructions of the same full-scale jet, and one that more readily accounts for geometrical spreading. Section II provides a brief review of the experiment. The methodology employed in the holography processing is described in Sec. III. First, compensation is made for a gap in the holography array. Second, similar to the approach of Long *et al.* (2009), a PFD of the measured jet data is performed using singular value decomposition (SVD) of the hologram cross spectral matrix (CSM). Third, due to the limited extent of the measurement array, the data are extrapolated numerically beyond the array boundaries using analytic continuation (Williams, 2003; see also Wall *et al.*, 2011b). Last, the data are propagated throughout the sound field with a cylindrical NAH method that is based on a discrete Fourier transform (Williams, 1999). Results from the PFD and NAH reconstruction are given in Sec. IV. Reconstructions are compared to benchmark measurements to show that this is an efficient method that provides an accurate reconstruction of the geometric near and mid fields, except in the far downstream region where the measurement aperture may not have extended far enough to sufficiently capture source energy. A key feature of the full-scale jet data—a double lobe in the radiated field—is demonstrated. Acoustic source distributions are shown. A summary of these results is given in Sec. V.

II. EXPERIMENT SUMMARY

Acoustical measurements from the installed engine on an F-22A Raptor were conducted in 2009 at Holloman Air Force Base in New Mexico (Wall *et al.*, 2012b). The engine closest to the measurement arrays was cycled through four power conditions: Idle, intermediate, military, and full afterburner, while the other engine was held at idle. The nozzle exit of each engine was centered 1.91 m above the ground and had a rectangular aspect ratio of approximately 1:2. During the static run-up measurements, the aircraft was tied down in the center of a 24.4 m (80 ft) wide concrete ground run-up pad.

The relative locations of the jet region and hologram measurement array are shown in Fig. 1. The origin of the coordinate system is on the ground directly below the nozzle exit. A stationary linear array of 50 microphones was placed along the surface of the concrete pad parallel to the centerline of the jet, or jet axis. These microphones, shown by the dots in Fig. 1, were placed on the ground 11.6 m (38.0 ft) from the centerline of the jet in the x-direction (11.7 m total distance in x and y) and spaced 0.61 m (2.0 ft) apart in the z-direction. There was a 1.5 m (5.0 ft) gap between the main microphone array and the last four microphones in the downstream region. With microphones on the rigid ground, multipath interference due to ground reflections was avoided. Several types of microphones were used in the measurement array including GRAS 6.35-mm (0.25-in) 40BD and 40BE pre-polarized microphones, 40BH externally polarized microphones, and GRAS 3.18-mm (0.125-in) 40DD pre-polarized microphones. The frequency ranges of the several microphone types are, respectively, 4 Hz to 70 kHz, 4 Hz to 80 kHz, 10 Hz to 20 kHz, and 6.5 Hz to 70 kHz. All microphones were laid out according to their sensitivities, taking into account the spatially dependent peak sound-pressure levels that were expected along the array.

A vertical planar region was measured about 4 m from and parallel to the approximate shear layer boundary. The measurement was made in a scan-based fashion with a dense, 90-microphone array, shown in Fig. 2(a). The bottom row of these measurements, which was 0.4 m from the ground, serves as a benchmark measurement for comparison

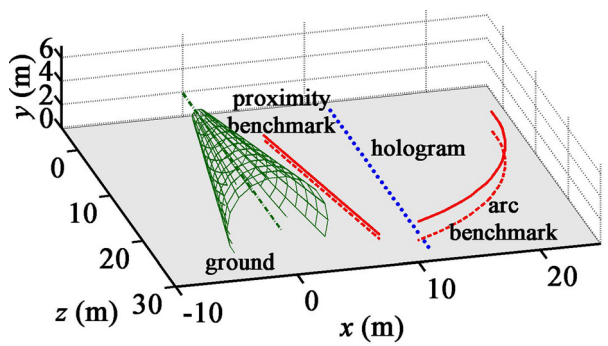

FIG. 1. (Color online) Schematic of the experimental setup. Relative locations of the approximate shear-layer region (represented by a cone), ground-based hologram measurement array (dotted line), and two benchmark measurement arrays (solid lines, with dashed lines to show their projected locations above the ground) are shown.

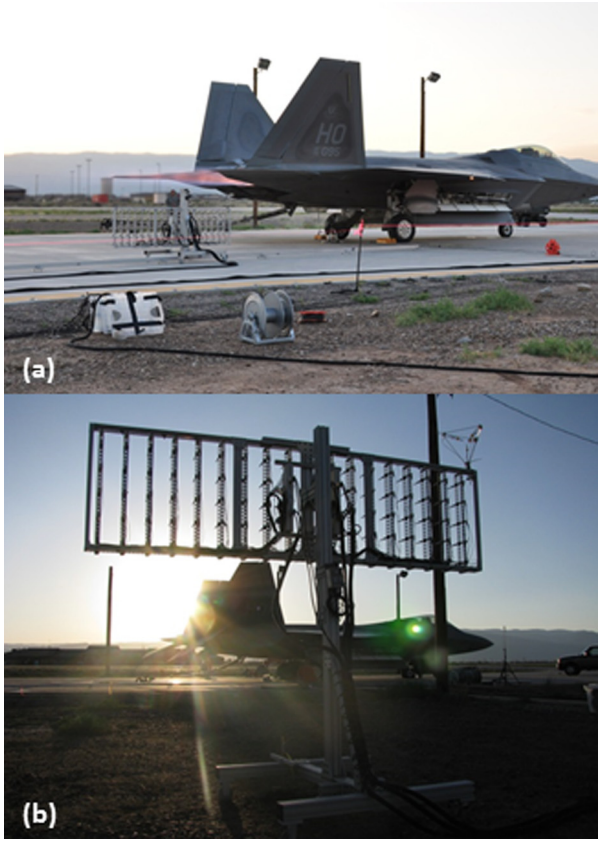

FIG. 2. (Color online) Images of the locations of the 90-microphone array in relation to the aircraft in the geometric (a) near field and (b) mid field. Scan-based near-field measurements were used for a benchmark in proximity to the jet, and the scan-based mid-field measurements were used for an additional benchmark.

with reconstructed levels. It is marked "proximity benchmark" in Fig. 1. In addition, an arc-shaped surface was measured (scan-based) in the transition region from the near to the far field by the same 90-microphone array, shown in Fig. 2(b). The arc was centered at a point 5.5 m (18.0 ft) downstream of the nozzle, with a radius of 22.9 m (75.0 ft). The location for the arc center is based on estimates of the maximum source region and corresponds to an arc center used by Gee *et al*. (2008). The data measured on the bottom row of the arc, which was 1.6 m from the ground, are also used as a benchmark, and their locations are marked "arc benchmark" in Fig. 1.

III. HOLOGRAPHY METHODOLOGY

A. Gap interpolation

It can be noted from the holography array marked by the dots in Fig. 1 that there was a gap of 1.5 m between the microphone near $z = 24.4$ m and the four microphones farthest downstream. In typical NAH measurements the last four microphones would not be used, since a discrete Fourier transform requires a regularly spaced array. However, the predictable, smoothly varying nature of the spatial sound field allowed the four downstream microphones to be employed to interpolate the measured field over the gap and maintain (estimate) regular (0.6 m) spacing.

For frequencies below about 160 Hz, a simple spline interpolation of the measured magnitudes and unwrapped phases (processed independently, then recombined afterward) is performed, starting with the existing array points and interpolating to regularly spaced locations that are a continuation of the main array in the downstream direction. Above 160 Hz, the unwrapped phases result in a discontinuity at the gap region. Subtraction of 2π from the unwrapped phases of the last four microphones prior to the interpolation serves to consistently remove the discontinuities for the frequencies of interest in this study that are above 160 Hz. For example, Fig. 3 shows the unwrapped phases measured along the array at 250 Hz for a set of complex pressures obtained from the Fourier transforms of the signals recorded during one simultaneous time block (dotted line) and the corresponding, phase-shifted, interpolated values (solid line).

B. PFD

A jet noise field is the result of radiation from multiple, ambiguous, partially coherent sources. Thus, the field is also partially coherent and must be represented by the superposition of multiple, mutually incoherent PFs. To do so requires first the measurement of multiple independent records of the field and the subsequent Fourier transform of each time record. The field cannot be uniquely determined from the Fourier transforms of a single block of time records obtained by the array, since coherence less than one cannot be represented by a single time harmonic field. Multiple time records are required to predict coherences of less than one.

To perform an NAH projection, the sound field must first be decomposed into a set of mutually incoherent PFs. The theory of principal component analysis is used in PFD techniques to generate a linearly independent basis set onto which the measured field can be projected. A PFD method based on the SVD (SPFD) of a CSM results in an optimal set of PFs, in that the most energy possible is partitioned into as few PFs as possible (Price and Bernhard, 1986). Each self-coherent PF can then be propagated individually with NAH, and their energetic sum produces the total reconstructed sound field. This SPFD was used by Hald (1989) to generate

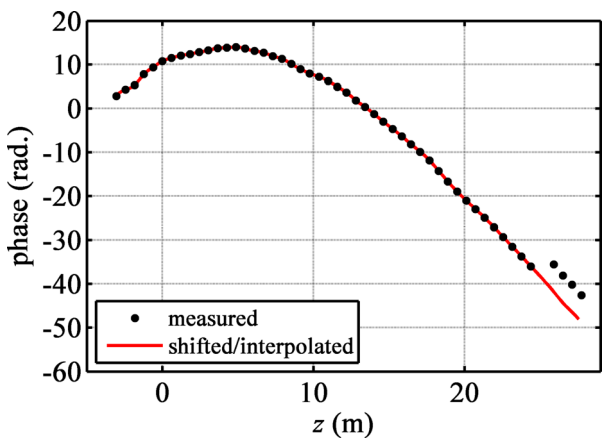

FIG. 3. (Color online) Unwrapped phases of the complex pressures along the measurement array for 250 Hz, and the corresponding interpolated, shifted phases.

mutually incoherent PFs from scan-based measurements in a holography method called Spatial Transformation of Sound Fields. Lee and Bolton (2006) expanded the SPFD to incorporate measurement noise and small variations in the source level, then applied the method to perform NAH on a laboratory scale jet (2007). The method by Lee and Bolton was also used by Wall *et al.* (2012a) to perform planar NAH reconstructions of a full-scale jet.

In SPFD, the measured sound field on the hologram array is represented by the matrix $\mathbf{P}=[\mathbf{p}_1\cdots\mathbf{p}_M]^{\mathrm{T}}$, where each row $\mathbf{p}_m$ is a vector that contains complex pressures obtained from the Fourier transform of multiple time histories measured at a single location of the M-element array, and T is the transpose operator. The CSM, $\mathbf{K}$, is calculated from $\mathbf{P}$ as

$$\mathbf{K}=\mathbf{P}\mathbf{P}^{\mathbf{H}}, \tag{1}$$

where H is the Hermitian transpose. Next, an eigenvalue decomposition (in the form of an SVD) of $\mathbf{K}$ in Eq. (1) is taken, giving

$$\mathbf{K}=\mathbf{U}\Sigma\mathbf{V}^{\mathbf{H}}. \tag{2}$$

Here, $\mathbf{U}$ and $\mathbf{V}$ are unitary matrices of the left and right singular vectors, respectively, which have normalized amplitude. (In this case, $\mathbf{U}=\mathbf{V}$ because the matrix $\mathbf{K}$ is positive semi-definite Hermitian.) The diagonal elements of the diagonal matrix, $\mathbf{\Sigma}$, are the singular values. Each singular value represents the autospectral amplitude of its corresponding singular vector. The PFs can be obtained with

$$\tilde{\mathbf{P}}=\Sigma^{1/2}\mathbf{U}^{\mathbf{H}}. \tag{3}$$

Because the SVD operation resulting in Eq. (2) provides PFs of monotonically decreasing magnitude, this allows a subset of the first N PFs to approximate the energy of all M PFs, expressed as

$$\tilde{\mathbf{P}}=[\mathbf{p}_1\ \cdots\ \mathbf{p}_M]^T\approx[\mathbf{p}_1\ \cdots\ \mathbf{p}_N\ \mathbf{0}\ \cdots\ \mathbf{0}]^{\mathrm{T}}. \tag{4}$$

The subset of PFs can be processed with NAH and the rest can be discarded. Since there is no distinct cutoff between the singular values related to source information and those related to noise in the case of a jet (Wall *et al.*, 2011a), the optimal selection of N in this preliminary "regularization" of the data is not well defined and merits further investigation. In the current work $N=10$ was found to be sufficient, in that, for all frequencies of interest, the addition of more PFs added negligible energy to the total field by visual inspection.

C. Numerical extrapolation of data

Following the PFD of the measured data, the aperture (spatial extent of the data in z) of each PF is extended numerically. Successful NAH reconstructions require that the hologram fully capture the important energy in the source region of interest. In addition, the aperture must be large enough to avoid the introduction of errors due to wraparound of the hologram data (Maynard *et al.*, 1985). If a hologram aperture is too small to avoid significant wraparound errors it may be helpful to numerically extend (extrapolate) the data into a region outside and tangent to the measurement surface, effectively increasing the aperture size. The extent to which aperture extension is successful depends on the method used and the available data. Analytic continuation is an extrapolation method that has been used to extend measured pressure fields into an area nearly double that of the original field, with high accuracy near the boundary of the original measurement (Williams, 2003). It is based on the Green's functions (transfer functions) relating acoustic quantities on the measurement surface to those on the extended surface. The use of analytic continuation has been explored as part of NAH investigations on the current full-scale jet noise data set (Wall *et al.*, 2011b; Wall *et al.*, 2012a).

As outlined by Williams (2003), the process of analytic continuation is as follows. First, the hologram data (here, each singular vector treated independently) are zero-padded. Second, the wavenumber spectrum is calculated through a discrete spatial Fourier transform. Third, the spectrum is filtered beyond a certain wavenumber cutoff, chosen during a modified Tikhonov regularization procedure (Williams, 2003). Fourth, an inverse Fourier transform is performed. Fifth, the filtered data in the locations of the original measurement are replaced with the original hologram data. This procedure is repeated iteratively until there is minimal change in the pressure values and the distribution is smooth, that is, until the L2 norm of the difference between iterations is less than the estimate of the noise variance times an *ad hoc* scaling factor (Williams, 2003) of 0.1. The result is a synthetic extended measurement aperture which estimates actual data near the original measurement boundary and transitions smoothly outward to low amplitudes. In this experiment, the field is extended about 60 m in both directions. An example of a continued field is provided in Sec. IV, and additional examples are given by Krueger (2012).

D. Sound field reconstruction

Once each PF has been numerically extended, they are projected with NAH. As mentioned previously, a long narrow sound source, such as a jet, is modeled by cylindrical wave functions more readily than planar functions. In cylindrical NAH (Williams, 1999), the general expression to extrapolate the field from the cylindrical shell $r=r_h$ to the shell $r=r_s$ is

$$p(r_s,\phi,z)=\sum_{n=-\infty}^{\infty}e^{jn\phi}\int_{-\infty}^{\infty}P_n(r_h,k_z)e^{jk_zz}\frac{H_n^{(1)}(k_rr_s)}{H_n^{(1)}(k_rr_h)}dk_z, \tag{5}$$

where $P_n(r_h,k_z)$ is the two-dimensional spatial Fourier transform in ϕ and z of the measured pressure at $r=r_h$, and $H^1{}_n(k_rr)$ is a Hankel function of the first kind defined by

$$H_n^{(1)}(k_rr)=J_n(k_rr)+jY_n(k_rr). \tag{6}$$

The functions J_n and Y_n are Bessel functions of the first and second kinds, respectively. The subscript n comes from the solution to the wave equation in cylindrical coordinates and is the separation of variables constant related to the azimuthal $\Phi(\phi)$ dependence. Evanescent waves are included in Eq. (5) since there are no restrictions on the values of k_r, allowing them to be real or imaginary.

Since the two-dimensional Fourier transform of the left-hand side of Eq. (5) is $P_n(r_s, k_z)$, then

$$P_n(r_s, k_z) = \frac{H_n^{(1)}(k_r r_s)}{H_n^{(1)}(k_r r_h)} P_n(r_h, k_z). \tag{7}$$

Equation (5) provides the relationship between the wave spectra at different cylindrical and planar surfaces. We call

$$G_p(r_s, r_h, k_r) = \frac{H_n^{(1)}(k_r r_s)}{H_n^{(1)}(k_r r_h)} \tag{8}$$

the pressure propagator and use it to propagate the pressure from one shell to another. The only restriction on r_s is that it be greater than or equal to the radius of the source. The radial wavenumber k_r is calculated by

$$k_r = \sqrt{k^2 - k_z^2}, \tag{9}$$

where k is the acoustic wavenumber, $k = 2\pi f/c$, f is the acoustic frequency (in hertz), and c is the fluid sound speed.

In the current work, the jet was measured in the presence of a rigid reflecting surface, i.e., a concrete run-up pad, and the microphone array was placed directly on that surface. This allows for an approximation of free-field conditions with an understanding that the pressure magnitude is approximately doubled at the hologram location. This requires an axisymmetric source assumption, or at least an acknowledgment of the fact that this reconstruction applies to a region covered by a limited azimuthal "slice" of the field in the direction of the measurement locations. Cylindrical NAH was applied to the (one-dimensional) extended PFs to reconstruct the sound field over a planar surface in z and r (radial distance from the jet centerline), as illustrated in Fig. 4. The azimuthal modes were thus limited to the $n = 0$ mode. Although several jet studies have demonstrated the relative importance of the first two or three azimuthal modes (Suzuki and Colonius, 2006; Michel, 2009; Tam *et al.*, 2010), it was not possible to calculate higher modes, because the hologram measurement was a one-dimensional array. The total reconstructed field is the energetic sum of all reconstructed PFs.

The reconstruction with cylindrical NAH is an approximation of a free-field measurement (with an approximately 6 dB level boost), but the benchmarks at other locations are influenced by frequency-dependent ground reflections. The arc and proximity measurements used as benchmark points were those limited to the bottom rows of the respective surfaces (see Fig. 1). A numerical experiment was performed to investigate the effect of interference due to ground reflections on the levels of the benchmark data. A single point source operating over the range of frequencies of interest in this paper was simulated at the height of the jet centerline and at the estimated maximum source region (center of the arc). SPLs were calculated at the same simulated locations as the two sets of benchmark measurements. Then, the simulation was repeated with the original point source and an additional image source below the ground-reflecting plane. The level difference between the two simulations at the same location was determined for the frequencies of interest. It was found that, for point sources, the level increase due to the presence of the reflecting plane (image source) was always between 4 and 6 dB, which approaches the 6 dB correction employed here. This point source model produces a more severe ground reflection effect than does an actual jet (Gee *et al.*, 2008). Since hologram and benchmark measurements each experienced quantitatively similar level increases, no alterations were made to levels presented in this paper to compensate for ground reflections.

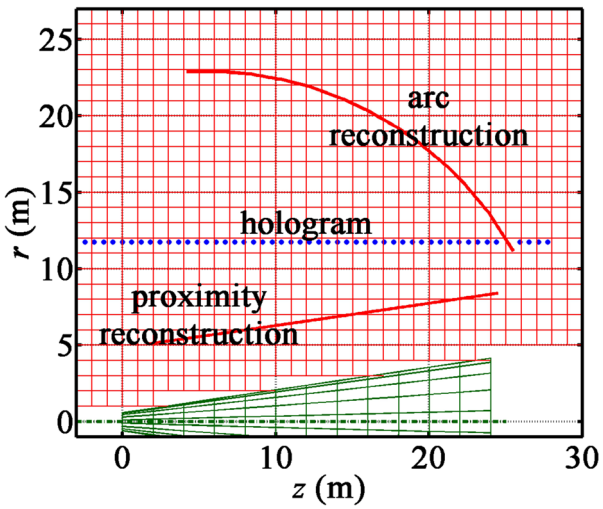

FIG. 4. (Color online) Diagram of the relative locations of the jet centerline (dashed line at $r = 0$), one-dimensional hologram array (dotted line) and the proximity and arc reconstruction locations (solid lines) in the two-dimensional reconstruction field (regular grid) set in the r - z coordinate system. Compare to Fig. 1.

IV. RESULTS

Results shown throughout this paper are all for measurements made with the engine operating at military powers. Frequencies of 63, 100, 200, and 250 Hz are investigated. The upper frequency used for NAH processing in this experiment is 250 Hz, because this approaches what might be considered a "spatial Nyquist frequency," where there are fewer than two microphones per acoustic wavelength, and the effects of spatial aliasing begin to corrupt the reconstructed data. The frequency 250 Hz is very near the characteristic frequency (frequency corresponding to the maximum level) of the radiation from large-scale turbulence structures for military powers (Wall *et al.*, 2012b), which radiation dominates the total field and is of particular interest in noise-reduction efforts.

In Fig. 5, levels measured by the holography array are shown for four frequencies as a function of distance

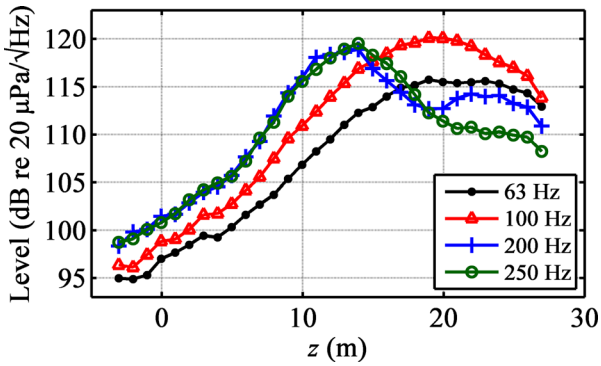

FIG. 5. (Color online) Measured levels (PSD) as a function of location along the holography array for 63, 100, 200, and 250 Hz.

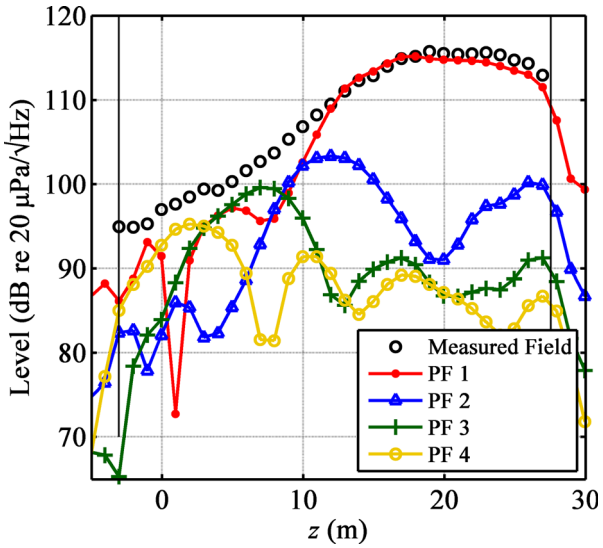

FIG. 6. (Color online) The first four PFs and the total field levels along the hologram at 63 Hz.

downstream, z. The levels are based on a power spectral density (PSD) calculation. The location of the maximum level shifts upstream (decreasing z) with increasing frequency, which demonstrates a frequency-dependent directionality of the source. Note also that the field magnitude varies smoothly over space, with broad distributions. The 200 Hz case is of particular interest. At this frequency, there is a two-lobe radiation pattern, shown by the double hump region of Fig. 5 from about $z = 10$ to 27 m. In a preliminary study by Tam and Parrish (2014), combustion noise was suggested as a possible mechanism for the generation of the second lobe. However, combustion noise would likely be localized at the nozzle exit, which is not seen in the present work or in recent phased-array analyses of the same data set (Harker *et al.*, 2014). Hence, further work is needed to investigate the cause of the two lobes, which are also present in other high-power military aircraft noise data sets (Norum *et al.*, 2004; McInerny *et al.*, 2007; Schlinker *et al.*, 2007; Gee *et al.*, 2005, 2008; Greska and Krothapali, 2008). Although the physical source mechanisms are difficult to evaluate due to the lack of flow data in the current data set, acoustic properties of the source are being investigated through the use of spatial coherence tools and the isolation of incoherent sources (Wall *et al.*, 2012c, 2013).

The PFD results are represented in Fig. 6 for an example frequency (63 Hz). The open circles mark the spatially dependent levels of the total field. The other four curves show the first four PFs, which are the singular vectors from the SVD scaled by their respective singular values [i.e., the first four rows of $\tilde{\mathbf{P}}$ from Eq. (3)]. The vertical lines mark the boundary of the actual measurement aperture; data shown beyond this boundary are the result of the analytic continuation of the PFs. First, note that the majority of the energy of the total field between about $z = 11$ and 27 m is captured in PF 1, and the additional PFs contribute more relative energy farther upstream. It is typical that jet noise fields at low frequencies (where large-scale turbulence radiation dominates) can be represented by relatively few PFs (Wall *et al.*, 2011a). More singular vectors are required to represent "sufficient energy" at higher frequencies (Vold *et al.*, 2012).

Figure 6 demonstrates a fundamental characteristic of SPFDs, which was investigated by Photiadis (1990). He showed how an SVD, when applied to simple geometries, resulted in nearly "modal" representations of sound fields analogous to sine/cosine waves on a string or modal patterns on a plate. The holography array in this experiment is one-dimensional and yields shapes similar to those observed by Photiadis. Note how PF 1 has a single characteristic maximum, PF 2 has two characteristic local maxima, PF 3 has three, and so on. This phenomenon occurs at all frequencies in the current experiment.

NAH reconstructions of the jet field are given in Fig. 7 for (a) 63 Hz and (b) 200 Hz. Levels are plotted as a function of distance downstream of the nozzle (z) and as a function of radial distance from the jet centerline (r). Reconstructed levels are shown up to, but not within, the approximate shear layer region. The locations of the array points are also shown by dots, for reference. The contour lines are placed 5 dB apart. With an increase in frequency the directionality of the radiation shifts toward the upstream direction as is demonstrated by the difference between the two frequencies shown here. Note that the 200 Hz case exhibits the two-lobe pattern demonstrated in Fig. 5, shown here by the two extended regions of high amplitude separated by a shallow null in Fig. 7(b). At both frequencies, the increase in level with decreasing distance from the source is qualitatively consistent with the geometrical spreading of radiation from a narrow extended source. This geometrical spreading is not easily represented in a plane wave NAH approach (Wall *et al.*, 2012a).

Reconstructed field levels at 63 Hz are compared to measured benchmark levels in Fig. 8. First, in Fig. 8(a), the levels are shown for the arc. The two curves agree within 2 dB at almost all locations. The levels at the proximity measurement are shown in Fig. 8(b). These agree to within 2 dB upstream of $z = 15$ m, but diverge downstream. This is likely due to the fact that the physical measurement aperture extended only to $z = 27.7$ m where the level only dropped about 3 dB below the maximum (see Fig. 5). The end of the array was not far enough downstream to capture sufficient energy in the radiated field, and the analytic continuation was not able to artificially restore (predict) this energy.

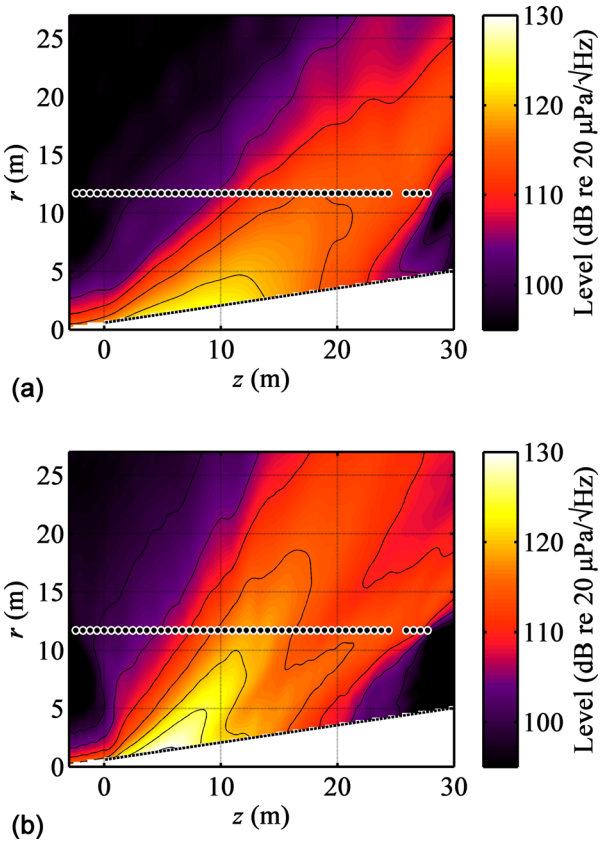

FIG. 7. (Color online) Jet-noise field reconstructions as a function of distance from the jet centerline (r) and distance downstream (z) for (a) 63 Hz and (b) 200 Hz.

Further evidence of this can be seen in the field reconstruction of Fig. 7(a). Here, the reconstructed levels along the measurement array (near $r = 12$ m) decrease gradually from about $z = 14$ to 27 m (the end of the array), but they decrease more rapidly downstream of this point. The downstream region of the arc is more accurately reconstructed, probably because the far downstream end of the arc approaches the hologram array, and the hologram array extends about 3 m beyond the end of the arc (see Fig. 1). This allows the array to capture most of the energy that is radiated toward the downstream region of the arc.

Similar benchmark comparisons for 200 Hz are shown in Fig. 9. Levels agree to within 2 dB at most points along the arc in Fig. 9(a) and in the upstream portion of the proximity measurement in Fig. 9(b), but they diverge downstream of $z = 15$ m near the jet. The same drop in level past the end of the holography array that was manifest in the 63 Hz case can be seen for 200 Hz in the downstream region of Fig. 7(b), suggesting that the array did not extend far enough downstream to capture all the important energy at 200 Hz. In addition, the double-lobe nature of the radiation at 200 Hz can more easily be seen by the double humps in these "slices" of the field shown in both parts of Fig. 9.

Reconstructed levels along the approximate shear layer boundary (marked by the boundary between the colored regions and the white regions in Fig. 7) are provided in Fig. 10 for the four frequencies of interest. The reconstruction of levels near the boundary of the shear layer provides an approximation of the jet noise source distributions. Near-source levels are shown as a function of z only. Based on the under-prediction of levels at the proximity benchmarks in Figs. 8 and 9, which were 4.1 m from and approximately parallel to the source reconstructions shown here, it is likely

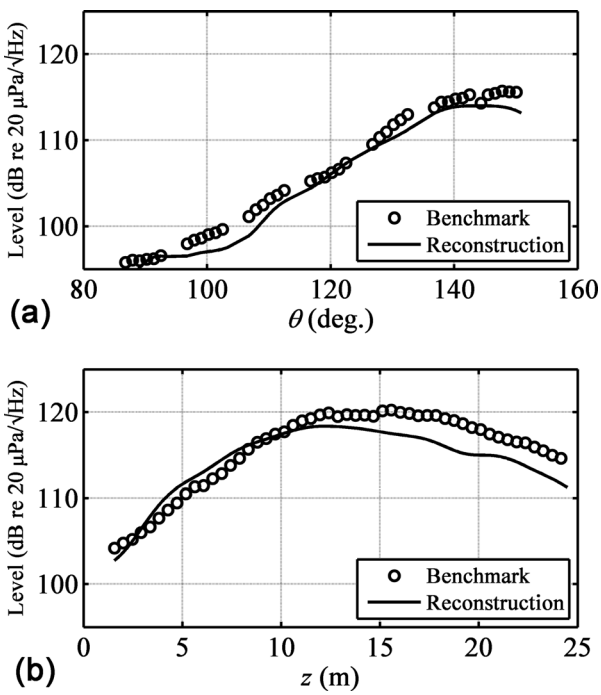

FIG. 8. Field reconstruction levels with comparisons to measured benchmarks for 63 Hz (a) at the arc location and (b) at the array nearest the shear layer.

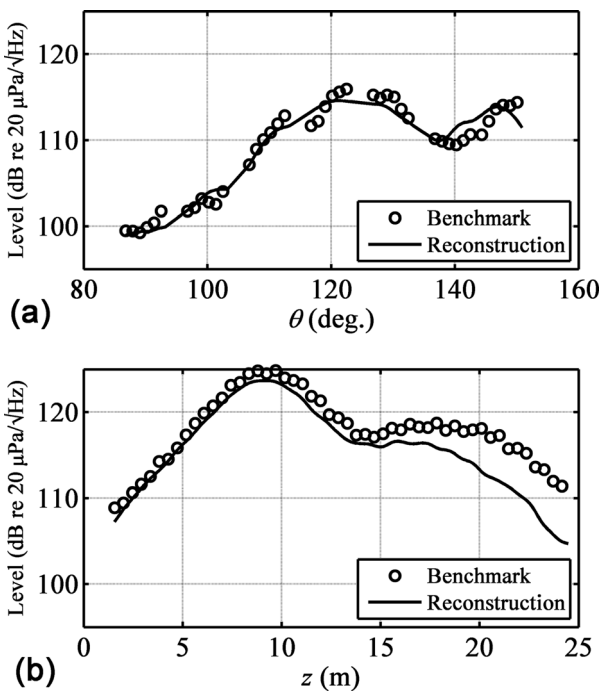

FIG. 9. Field reconstruction levels with comparisons to measured benchmarks for 200 Hz (a) at the arc location and (b) at the array nearest the shear layer.

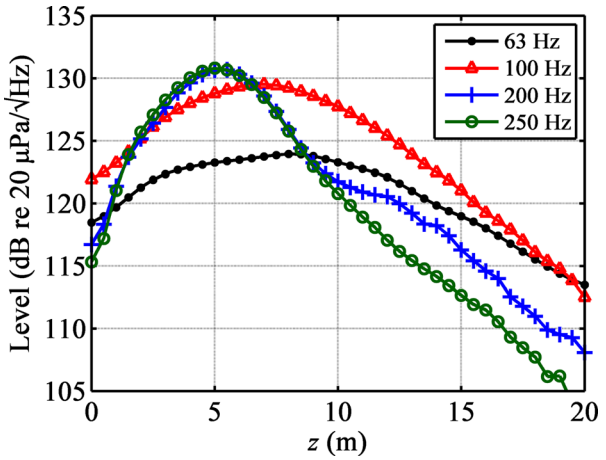

FIG. 10. (Color online) Reconstructed level distributions (equivalent sources) along the approximate shear layer location.

that source levels are under-predicted downstream of about $z = 10$ or 15 m. Source regions of higher frequencies tend to originate farther upstream, and have narrower distributions, than those of the lower frequencies. This is consistent with laboratory-scale phased-array measurements of both hot and cold, subsonic and supersonic jets (Lee and Bridges, 2005). However, Schlinker *et al.* (2007) showed that the source peak location of a full-scale jet, measured with a phased-array method, was highly independent of frequency. Further investigation is required to address these differences. Note also that the 200 and 250 Hz peak distributions are nearly identical. The broader "hump" in the 200 Hz distribution, between $z = 10$ and 15 m, is caused by the presence of the secondary lobe in the radiated field. This suggests the existence of two spatially distinct source regions for the two radiation lobes [compare Fig. 7(b)]. Since the hump is not present in the 250 Hz curve, the secondary lobe is likely diminishing as frequency increases above 200 Hz.

Source distributions in Fig. 10 can be compared to those obtained from the planar NAH experiment performed for the same full-scale jet previously (see Figs. 9 and 11 of Wall *et al.*, 2012a). In that study reconstructed levels were predicted over a planar region that ran parallel (and tangent) to the edge of the shear layer boundary, for frequencies of 105 and 210 Hz, which are close to the frequencies 100 and 200 shown here. Planar NAH predictions locate the source distribution maxima near 7–8 m and 5–6 m for 105 and 210 Hz, respectively, which are the same locations for the 100 and 200 Hz curves of Fig. 10. The two sets of distribution shapes are also quantitatively similar.

V. CONCLUDING DISCUSSION

NAH measurements of full-scale jets can require a prohibitively large number of measurements and considerable resources. Additional complexity is introduced by the necessity of accounting for the presence of ground reflections in measured data. It has been shown in this paper that cylindrical NAH with a one-dimensional array of microphones on the ground is an efficient and convenient way to measure the field and estimate radiated levels from the simplest sources—which radiate at the low frequencies and dominate the total field—of a full-scale jet. The reconstructions shown in this paper have been able to qualitatively represent frequency-dependent level distributions near the jet shear layer boundary and radiation patterns, which are consistent with previously laboratory-scale data. The approximations of source distributions given here are quantitatively consistent with those generated in a previous planar NAH experiment for the same data set, and can be compared to those produced from other methods in the future. In addition, evidence was demonstrated here of jet noise source radiation in a double-lobe pattern near 200 Hz, which is commonly present in high-power military jets, and is the subject of ongoing investigation. In regions of the sound field where the measurement aperture sufficiently captured the radiated energy, reconstructions were within 2 dB of measured benchmark levels, with an accurate representation of spatial trends. This is true in spite of the fact that the nozzle was rectangular. It is important to understand that the measurements and reconstructions all occurred within a relatively small azimuthal aperture window. Greater azimuthal coverage would be necessary to represent non-axisymmetric features of a jet, including those of the current jet. Future measurements would likely benefit by extending the holography array several meters farther downstream to ensure that sufficient radiation energy is captured within the axial aperture.

ACKNOWLEDGMENTS

The authors gratefully acknowledge funding from the U.S. Air Force Research Laboratory (USAFRL) through the SBIR program and support through a Cooperative Research and Development Agreement between Blue Ridge Research and Consulting, Brigham Young University, and the Air Force. The authors also recognize the contributions of Richard McKinley and Robert McKinley with the USAFRL. This research was supported in part by the appointment of A.T.W. to the Student Research Participation Program at USAFRL, Human Effectiveness Directorate, Warfighter Interface Division, Battlespace Acoustics administered by the Oak Ridge Institute for Science and Education through an interagency agreement between the U.S. Department of Energy and USAFRL. Distribution A: Approved for public release; distribution unlimited. 88ABW Cleared March 13, 2014; 88ABW-2014-1040.

Arndt, R. E. A., Long, D., and Glauser, M. (**1997**). "The proper orthogonal decomposition of pressure fluctuations surrounding a turbulent jet," J. Fluid Mech. **340**, 1–33.

Fuchs, H. V., and Michel, U. (**1978**). "Experimental evidence of turbulent source coherence affecting jet noise," AIAA J. **16**, 871–872.

Gee, K. L., Gabrielson, T. B., Atchley, A. A., and Sparrow, V. W. (**2005**). "Preliminary analysis of nonlinearity in military jet aircraft noise propagation," AIAA J. **43**, 1398–1401.

Gee, K. L., Neilsen, T. B., Wall, A. T., Downing, J. M., and James, M. M. (**2013**). "The 'sound of freedom': Characterizing jet noise from high-performance military aircraft," Acoust. Today **9**(**3**), 8–21.

Gee, K. L., Sparrow, V. W., James, M. M., Downing, J. M., Hobbs, C. M., Gabrielson, T. B., and Atchley, A. A. (**2008**). "The role of nonlinear effects in the propagation of noise from high-power jet aircraft," J. Acoust. Soc. Am. **123**, 4082–4093.

Greska, B., and Krothapalli, A. (**2008**). "On the far-field propagation of high-speed jet noise," in *Proceedings of NCAD/NOISE-CON*.

Hald, J. (**1989**). "STSF—A unique technique for scan-based nearfield acoustical holography without restriction on coherence," Technical Report No. 1 (Bruel & Kjaer, Naerum, Denmark).
Harker, B. M., Gee, K. L., Neilsen, T. B., Wall, A. T., and James, M. M. (**2014**). "Phased-array measurements of full-scale military jet noise," AIAA Paper 2014-3069 (Atlanta, GA).
Harker, B. M., Gee, K. L., Neilsen, T. B., Wall, A. T., McInerny, S. A., and James, M. M. (**2013**). "On autocorrelation analysis of jet noise," J. Acoust. Soc. Am. **133**(6), EL458–EL464.
Krueger, D. W. (**2012**). "Array-based characterization of military jet aircraft noise," Master's thesis, Brigham Young University.
Kuo, C.-W., Buisson, Q., McLaughlin, D. K., and Morris, P. J. (**2013**). "Experimental investigation of near-field pressure fluctuations generated by supersonic jets," AIAA Paper 2013-2033 (Berlin, Germany).
Lee, M., and Bolton, J. S. (**2006**). "Scan-based near-field acoustical holography and partial field decomposition in the presence of noise and source level variation," J. Acoust. Soc. Am. **119**, 382–393.
Lee, M., and Bolton, J. S. (**2007**). "Source characterization of a subsonic jet by using near-field acoustical holography," J. Acoust. Soc. Am. **121**, 967–977.
Lee, S. S., and Bridges, J. (**2005**). "Phased-array measurements of single flow hot jets," AIAA Paper 2005-2842 (Monterey, CA).
Long, D., Peters, J., and Anderson, M. (**2009**). "Evaluating turbofan exhaust noise and source characteristics from near field measurements," AIAA Paper 2009-3214 (Miami, FL).
Maynard, J. D., Williams, E. G., and Lee, Y. (**1985**). "Nearfield acoustic holography: 1. Theory of generalized holography and the development of NAH," J. Acoust. Soc. Am. **78**, 1395–1413.
McInerny, S. A., Gee, K. L., Downing, J. M., and James, M. M. (**2007**). "Acoustical nonlinearities in aircraft flyover data," AIAA Paper 2007-3654 (Rome, Italy).
McInerny, S. A., Lu, G., and Olcmen, S. (**2004**). "Rocket and jet mixing noise, background and prediction procedures," Report for National Center for Physical Acoustics, University of Mississippi.
Michalke, A. (**1977**). "On the effect of spatial source coherence on the radiation of jet noise," J. Sound Vib. **55**, 377–394.
Michel, U. (**2009**). "The role of source interference in jet noise," AIAA Paper 2009-3377 (Miami, FL).
Norum, T. D., Garber, D. P., Golub, R. A., Santa Maria, O. L., and Orme, J. S. (**2004**). "Supersonic jet exhaust noise at high subsonic flight speed," NASA TP 212686.
Otte, D., Sas, P., and Ponseele, P. V. (**1988**). "Noise source identification by use of principal component analysis," in *Proceedings Inter-Noise* 88, p. 199.
Photiadis, D. M. (**1990**). "The relationship of singular value decomposition to wave-vector filtering in sound radiation problems," J. Acoust. Soc. Am. **88**(2), 1152–1159.
Price, S. M., and Bernhard, R. J. (**1986**). "Virtual coherence: A digital signal processing technique for incoherent source identification," in *Proceedings of the 4th International Modal Analysis Conference*, pp. 1256–1262.
Schlinker, R. H., Lijenberg, S. A., Polak, D. R., Post, K. A., Chipman, C. T., and Stern, A. M. (**2007**). "Supersonic jet noise source characteristics & propagation: Engine and model scale," AIAA Paper 2007-6023 (Long Beach, CA).
Shah, P. N., Vold, H., and Yang, M. (**2011**). "Reconstruction of far-field noise using multireference acoustical holography measurements of high-speed jets," AIAA Paper 2011-2772 (Portland, OR).
Suzuki, T., and Colonius, T. (**2006**). "Instability waves in a subsonic round jet detected using a near-field phased microphone array," J. Fluid Mech. **565**, 197–226.
Tam, C. K. W., and Parrish, S. A. (**2014**). "Noise of high-performance aircrafts at afterburner," AIAA Paper 2014-2754 (Atlanta, GA).
Tam, C. K. W., Pasouchenko, N. N., and Schlinker, R. H. (**2006**). "Noise source distribution in supersonic jets," J. Sound Vib. **291**, 192–201.
Tam, C. K. W., Viswanathan, K., Pastouchenko, N. N., and Tam, B. (**2010**). "Continuation of the near acoustic field of a jet to the far field. Part II: Experimental validation and noise source characteristics," AIAA Paper 2010-3729 (Stockholm, Sweden).
Viswanathan, K. (**2007**). "Investigation of the sources of jet noise," AIAA Paper 2007-3601 (Long Beach, CA).
Vold, H., Shah, P., Morris, P., Du, Y., and Papamoschou, D. (**2012**). "Axisymmetry and azimuthal modes in jet noise," AIAA Paper 2012-2214 (Colorado Springs, CO).
Wall, A. T., Gee, K. L., Gardner, M. D., Neilsen, T. B., and James, M. M. (**2011a**). "Near-field acoustical holography applied to high-performance jet aircraft noise," Proc. Meet. Acoust. **9**, 040009.
Wall, A. T., Gee, K. L., James, M. M., Bradley, K. A., McInerny, S. A., and Neilsen, T. B. (**2012b**). "Near-field noise measurements of a high-performance military jet aircraft," Noise Control Eng. J. **60**, 421–434.
Wall, A. T., Gee, K. L., Krueger, D. W., Neilsen, T. B., Sommerfeldt, S. D., and James, M. M. (**2011b**). "Aperture extension for near-field acoustical holography of jet noise," Proc. Meet. Acoust. **14**, 065001.
Wall, A. T., Gee, K. L., Neilsen, T. B., and James, M. M. (**2012c**), "Partial field decomposition of jet noise sources using optimally located virtual reference microphones," Proc. Meet. Acoust. **18**, 045001.
Wall, A. T., Gee, K. L., Neilsen, T. B., and James, M. M. (**2013**). "Acoustical holography and proper orthogonal decomposition methods for the analysis of military jet noise," in *Proceedings of NOISE-CON 2013*, Denver, CO.
Wall, A. T., Gee, K. L., Neilsen, T. B., Krueger, D. W., James, M. M., Sommerfeldt, S. D., and Blotter, J. D. (**2012a**). "Full-scale jet noise characterization using scan-based acoustical holography," AIAA Paper 2012-2081 (Colorado Springs, CO).
Williams, E. G. (**1999**). *Fourier Acoustics: Sound Radiation and Nearfield Acoustical Holography* (Academic Press, San Diego, CA), pp. 149–182.
Williams, E. G. (**2001**). "Regularization methods for near-field acoustical holography," J. Acoust. Soc. Am. **110**, 1976–1988.
Williams, E. G. (**2003**). "Continuation of acoustic near-fields," J. Acoust. Soc. Am. **113**, 1273–1281.